

Treating High Energy Showers

Alfredo Ferrari and Paola R. Sala

Istituto Nazionale di Fisica Nucleare, Sezione di Milano
Via Celoria 16, 20133 Milano, Italy

Lecture given at the

*Training Course on the Use of MCNP in Radiation Protection
and Dosimetry*

Bologna - Italy, may 13–16 1996

Proceedings in press

Treating High Energy Showers

Alfredo Ferrari, and Paola R. Sala

INFN, Sezione di Milano, Via Celoria 16, 20133 Milano, Italy

Abstract

Some features of hadronic showers in the energy range from a few tens of MeV up to several hundreds GeV, are presented, with particular emphasis on general properties and scaling properties.

Examples of performances of state-of-the-art nuclear models are also given.

1 Introduction

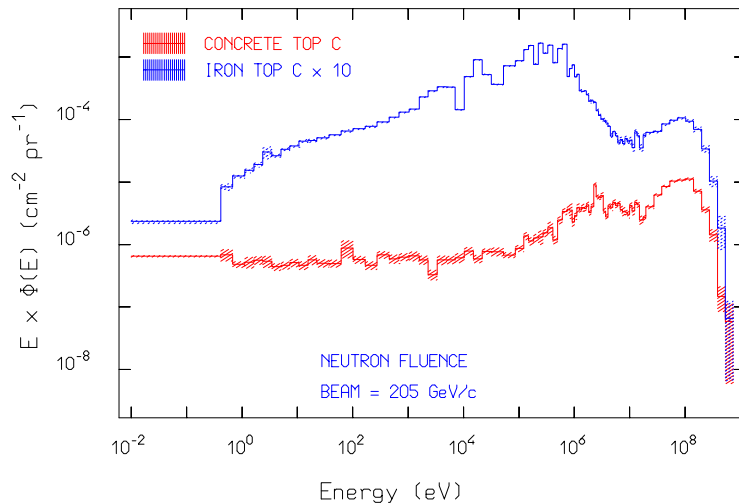


Figure 1: Neutron fluence resulting from calculations for the concrete top and iron top positions of the CERN-CEC facility for high energy dosimetry [1]

The importance of shower simulations in many fields of present day particle physics has grown considerably during the last years, in parallel with the rapid increase in available CPU power.

Besides physics experiment, there is an increasing interest for applications of accelerator beams. A new generation of intermediate energy proton and electron accelerators is under construction or planned in the near future, spanning a variety of applications, ranging from energy production, waste transmutation, synchrotron radiation to radiotherapy. Such applications call

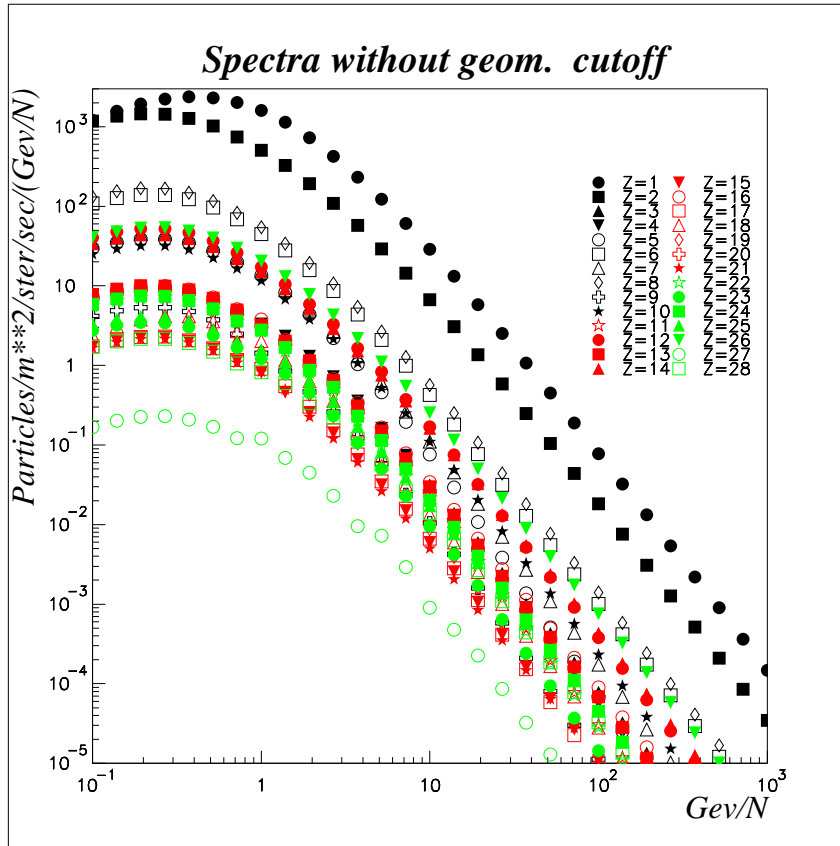


Figure 2: Cosmic ray fluences with no geomagnetic cutoffs

for more and more refined simulations tools, to be able to design and properly operate these facilities. Examples of the neutron spectra emerging from the lateral shielding of a high energy accelerators are presented in fig. 1. These computed spectra (which have been extensively checked with experimental measurements [1]) refer to the concrete and iron shielding positions of the CERN-CEC facility for high energy neutron dosimetry.

A good knowledge of radiation transport is critical also for other activities which apparently have very little in common with the new medical and industrial accelerators. Radiation background in the large experiments which are currently planned to be installed at the future LHC proton-proton collider will be dominated by particle fluxes which can only be estimated by simulation of the whole hadronic cascade from several TeV down to thermal energies. Most of the particle production will take place at energies below 1 GeV.

A similar situation arises in the assessment of the radiation dose affecting the crew of commercial airplanes or of space stations, where the capabilities of understanding the radiation environment generated by cosmic rays is of utmost importance. The spectra of cosmic rays impinging on the earth atmosphere are shown in figs. 2 and 3 for no geomagnetic shield and for an

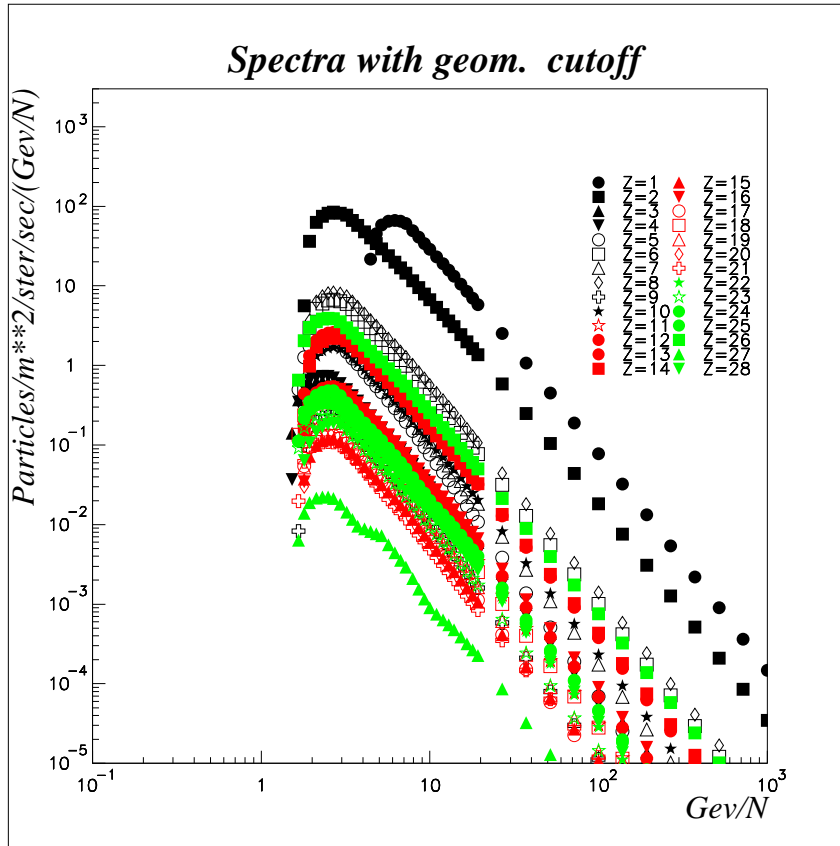


Figure 3: Cosmic ray fluences for an intermediate geomagnetic latitude

intermediate latitude respectively. It is apparent from these spectra that good physics modelling is required from few MeV up to several tens of GeV at least.

In general all aspects connected with the dosimetry of medium and high energy particles are still waiting for a fresh and more systematic treatment.

Detailed physical models are also required when designing and operating experiments based on calorimetry. Missing p_t measurements and CP violation experiments are very sensitive to the response of calorimeters to relatively low energy hadrons. A detailed comprehension of active device responses to subGeV hadrons will be a key issue for many of the future experiments, both at accelerator beams, or in underground laboratories. Despite they heavily rely on MonteCarlo modelling when designing and understanding their devices, and when analyzing experimental data for backgrounds and kinematical cuts, high energy physicists tend to consider all the complex phenomena of hadronic and electromagnetic showers occurring in their experimental apparatus as well understood physics, without recognizing the still large uncertainties connected with the physical description of showers. While QCD inspired models are very powerful in predicting and describing the rare interesting phenomena searched for by high energy experiments,

efforts in describing the bulk of high energy interactions, which cannot be understood in terms of perturbative QCD, are relatively rare, despite their striking importance in understanding the complex experimental setups required by modern experiments.

Nuclear physicists are often working on a small subset of “interesting” phenomena related to nuclear interactions, and usually do not like to spend time on more general models which can be used for whichever application, particularly for technological ones. Very interesting physics researches are going on in the description of nucleon induced interactions below the pion threshold (see the reviews [2, 3]), however little or no work is done in the understanding of interactions at higher energies, with possibly the exception of some interesting developments in the pion sector [4, 5, 6]. Anyway, new or updated models are seldom formulated in such a way as to allow a general application. As a consequence, most applications must rely on models, like the glorious Bertini INC model, which are 20 to 30 years old, and which are no longer up-to-date with the present knowledge.

As soon as the energy of a primary hadron beam exceeds few tens of MeV, inelastic interactions start to play a major role and secondaries have enough energies to trigger further interactions, giving rise to a hadronic shower. Whenever the beam energy is such that significant pion production can occur (the pion production threshold for nucleons interacting with stationary nucleons is around 290 MeV), an increasing fraction of the energy is transferred from the hadronic (HAD) to the electromagnetic (EM) sector due to production of mesons (mainly π^0 and η) which quickly decay into EM particles (e^+ , e^- , and γ). Hadron and electromagnetic showers are very complex phenomena, whose description in terms of basic physical interactions requires a lot of knowledge. There are two basic differences between hadronic and EM showers. The first is that, while energetic hadronic showers are always giving rise to significant EM ones (and we shall see in section 4 how such EM component is more and more important with increasing primary energy), EM showers develop independently without further hadronic particle production, forgetting for a while the (small) probability of electro and photonuclear interactions. The second difference is that, while EM interactions are in principle well understood (see however [7]) and described by QED, the same does not apply to hadronic nuclear interactions, where such a complete theory does not exist and one has to resort to suitable models to have some insight into the physics of the processes.

The development of hadron initiated showers is determined both by atomic processes (dE/dx , multiple Coulomb Scattering etc), which take place very frequently, and by the relatively rare nuclear interactions (both elastic and nonelastic). EM showers are determined by the same atomic processes (dE/dx , multiple Coulomb Scattering etc), plus other atomic processes (Bremsstrahlung, pair production, Compton scattering etc), which are specific of e^\pm and photons, while nuclear interactions play a minor role, and whenever the interest is not in the small amount of hadrons produced by EM particles, they can be safely neglected.

A simple and schematic description of shower development is presented in section 2. The atomic processes common to HAD and EM showers are not treated in this lecture (see [8, 9, 10, 11, 12, 13]). Only a “macroscopical” description of hadronic showers will be given, while a description of hadron-nucleus interactions can be found in [14] and references therein. Finally a short introduction to EM showers is presented in section 4.

Before going on with the proposed scheme, it is important to make the reader aware of a few important warnings and comments. The present lecture is based on the experience and feelings of the authors, who work since several years in the field of shower modelling, mainly for applications connected with high energy accelerators and experiments. Their opinions are not necessarily those of the majority of people working in the field.

Whenever presented, plots of cross sections etc are to be intended as indicative. Usually the data used for such plots are taken from the tabulations used by the author code (FLUKA). Whenever experimental data are plotted, the source is always indicated. Most of the examples have been computed again with FLUKA, just for convenience: indications whether they can be considered or not as typical examples are given every time.

No discussion is given about hadron (neutron) interactions below, say, 20 MeV, both because they are outside the aim of this lecture, and because they are essentially restricted to neutron interactions, for which a huge and accurate body of experimental informations, sometimes supplemented by sophisticated modelling does exist in official compilations like ENDF-B, JEF, JENDL etc. It is always assumed that (neutron) interactions below 20 MeV can be accurately simulated with the codes developed for this energy range [15, 16, 17], which make use of such informations.

2 Shower Development

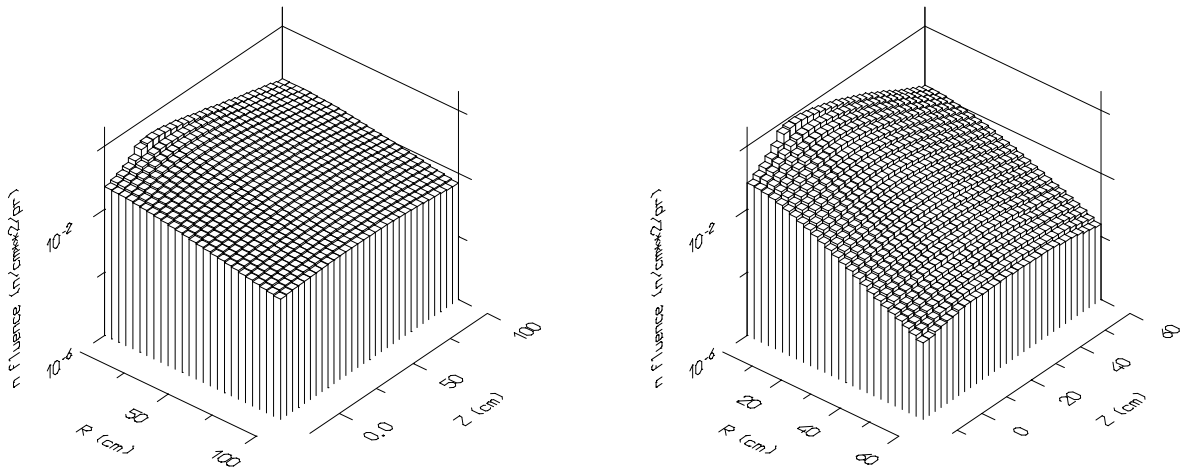


Figure 4: Spatial distribution of neutron fluence in an infinite natural Pb (left) and depleted U (right) target, for a 1.5 GeV incident proton beam

Before discussing specific aspects of hadronic and EM showers, there are a few comments which help in focusing the problem. Assuming one is dealing with some technological application of

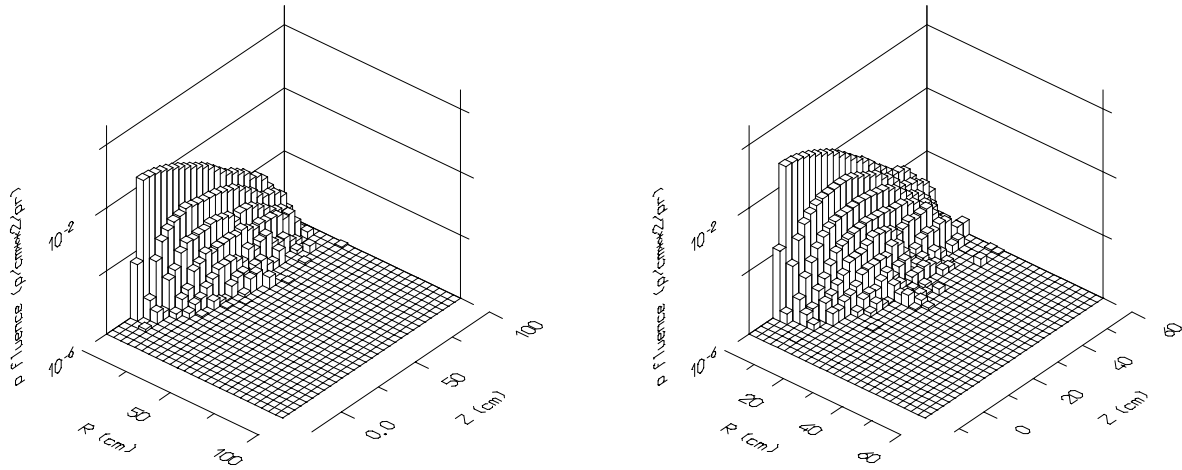


Figure 5: Spatial distribution of proton fluence in an infinite natural Pb (left) and depleted U (right) target, for a 1.5 GeV incident proton beam

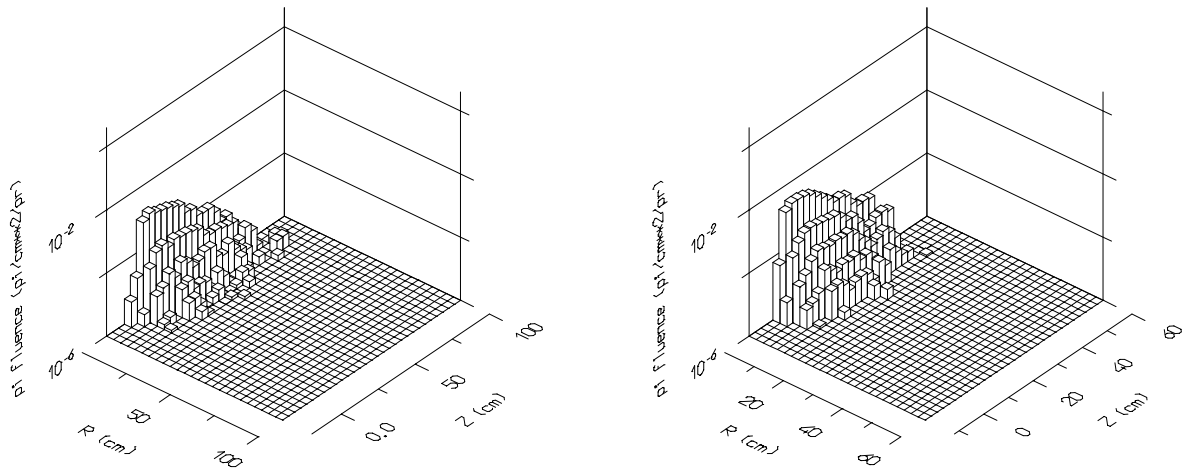


Figure 6: Spatial distribution of charged pion fluence in an infinite natural Pb (left) and depleted U (right) target, for a 1.5 GeV incident proton beam

an accelerator beam (energy production, waste transmutation, cancer therapy etc), which kind of informations does he need? Without claiming that these are all the possible informations required, a reasonable list could be the following:

- Energy deposition (with possibly the chance to weight energy deposition according to the “depositing” particle/process, as required for example for biological effectiveness evaluation and for radioprotection)

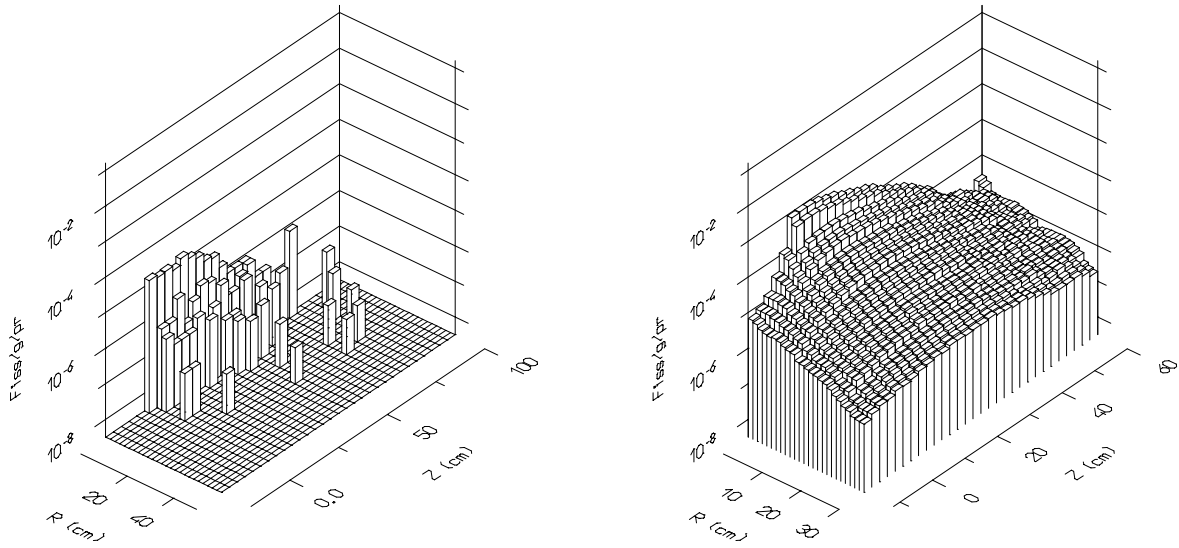


Figure 7: Spatial distribution of fission density in an infinite natural Pb (left) and depleted U (right) target, for a 1.5 GeV incident proton beam

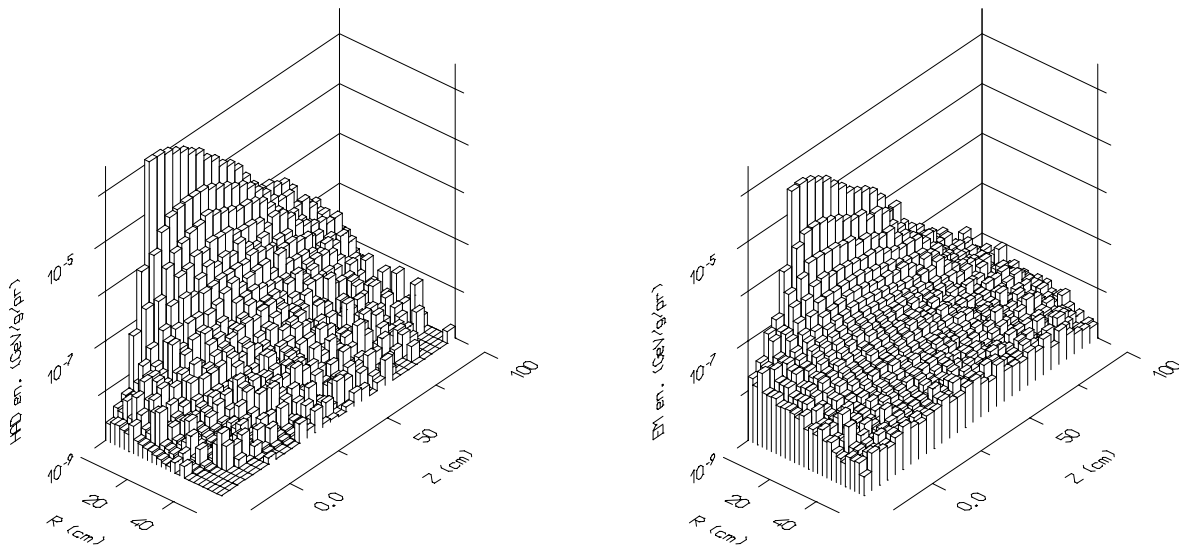


Figure 8: Hadronic (left) and EM (right) energy density distribution in an infinite natural Pb target, for a 1.5 GeV incident proton beam

- Particle fluences as a function of energy, angle and position
- Interaction distributions (inelastic interaction density, fission density etc)
- Residual nuclei, that is the (possibly radioactive) isotopes generated by beam interactions in the target

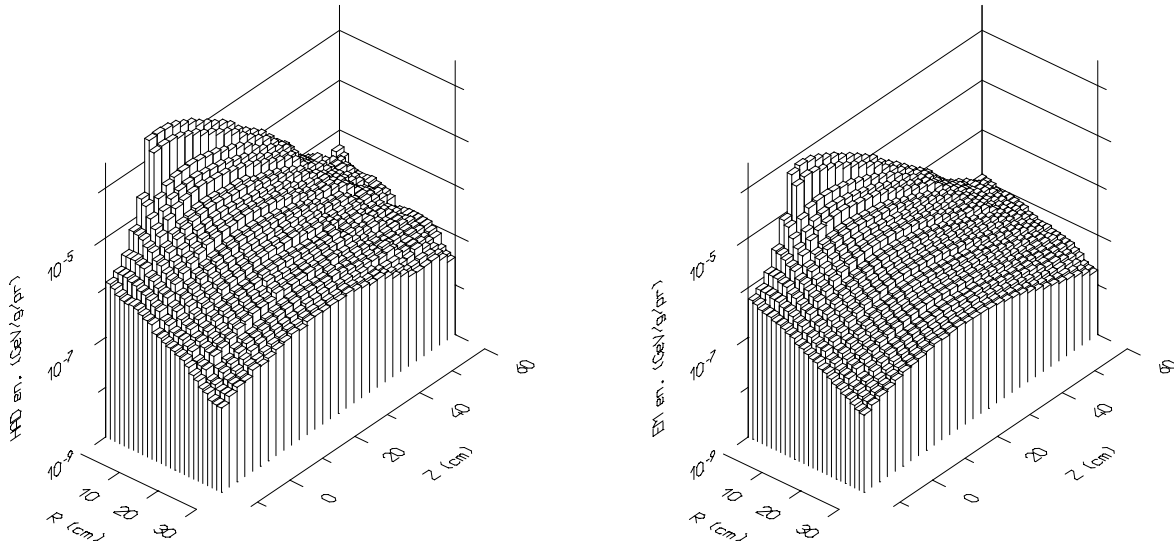


Figure 9: Hadronic (left) and EM (right) energy density distribution in an infinite natural U target, for a 1.5 GeV incident proton beam

Ideally, our tool, from now identified with some MonteCarlo program, should be able to give us accurate predictions about all the above points, for any desired spatial mesh. Usually the degree of accuracy required for the different kind of informations is not the same. For example, residual nuclei are seldom required to an accuracy better than one order of magnitude, while neutron fluences can well be requested to be within a factor 10% or better.

2.1 HAD shower examples

As an example of the development of hadronic showers, and at the same time of the kind of informations which can be obtained by modern MonteCarlo codes, let us consider a 1.5 GeV proton beam impinging at the coordinate origin on infinite natural lead and depleted uranium (0.2% ^{235}U) targets. These targets have been selected because most of the proposed technological applications of accelerator beams will make use of heavy (and possibly fissionable) targets. In fig. 4,5,6, the spatial distribution of neutron, protons, and charged pion fluences in both targets are presented, while the fission distributions are shown in fig. 7. The Z and R axis have been rescaled in such a way as to cover the same “length” for the two targets when expressed in g/cm^2 , in order to mask every difference due to the different densities. The hadronic and EM energy densities (the last due to π^0 's, capture photons etc) are plotted in fig. 8 and 9 for the Pb and U target respectively.

There are similarities and striking differences between the two targets, which need a bit of discussion. Proton and pion fluence distributions look very similar both in shape and in absolute value. They are both concentrated close to the primary beam axis, as expected since they originate mainly from energetic particles which, by virtue of momentum conservation and of

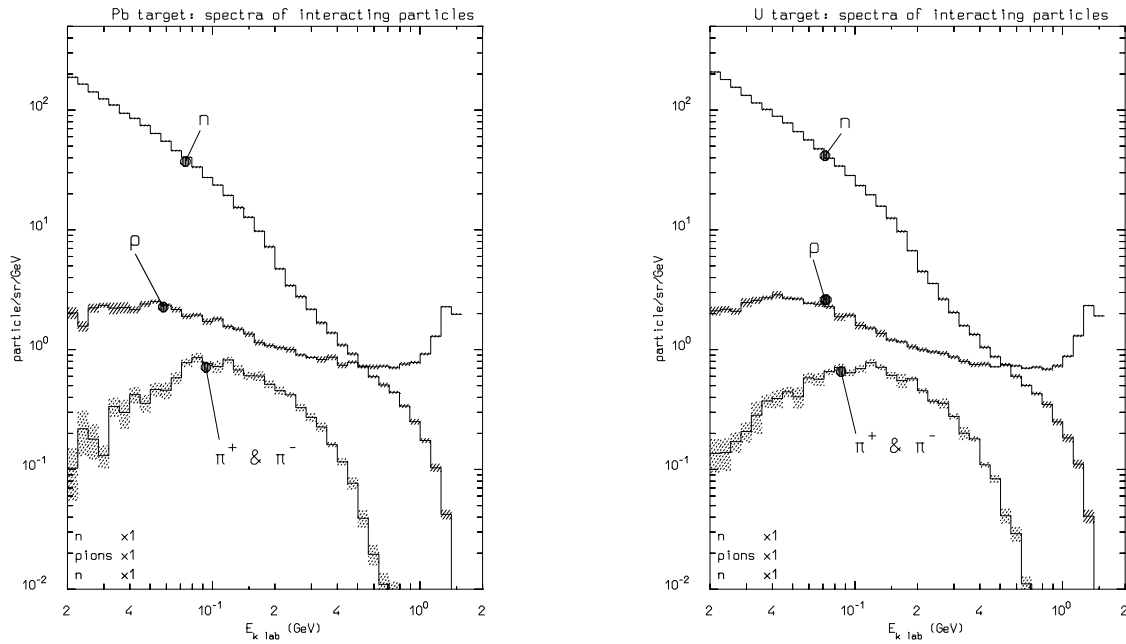


Figure 10: Spectra of p,n, and pions undergoing nuclear interactions in an infinite natural U (right) and Pb (left) target, for a 1.5 GeV incident proton beam

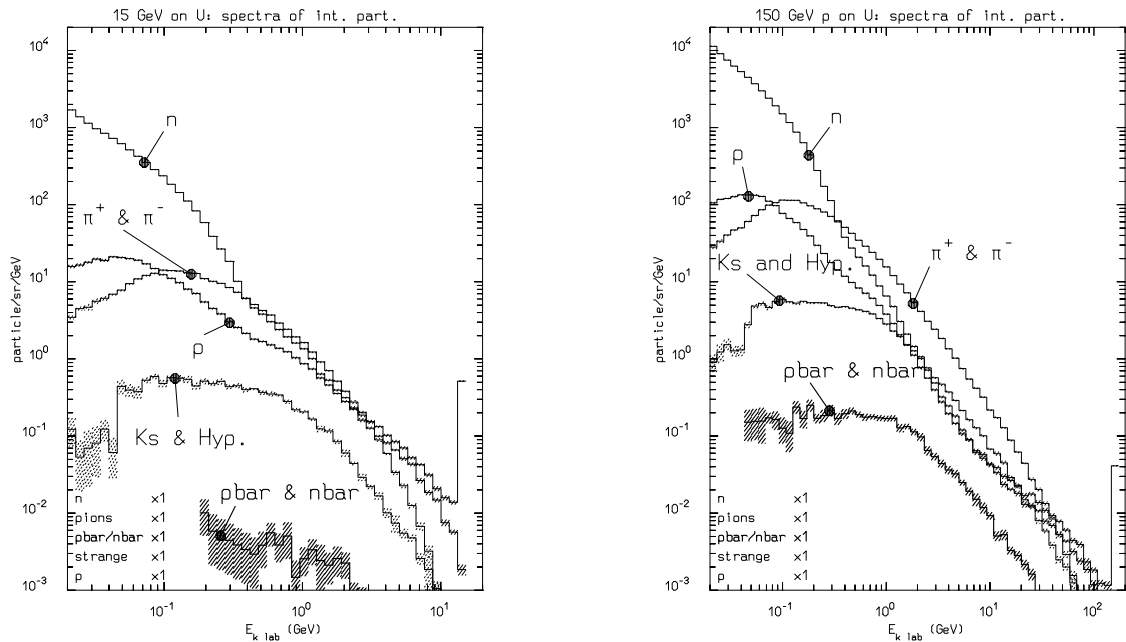


Figure 11: Spectra of particles undergoing nuclear interactions in an infinite natural U for 15 GeV (left) and 150 (right) incident proton beam. Note the different scale with respect to the previous figures

the forward asymmetry in most center of mass angular distributions, are strongly peaked in the original direction. The proton distribution is higher and wider than the pion one, because protons can be produced also during the final evaporation stage and by particles of relatively low energy, while the threshold for pion production is much higher. The number of neutrons is much big-

ger, and spread over a much larger volume. The faster decrease of neutron fluence with radius in the U target is just due to the larger absorption than in the Pb target. To better understand the role of different particles/energies in determining the shower evolution, it is interesting to look at the spectra of particle undergoing nuclear inelastic interactions. These spectra are shown in fig. 10 for both targets. The peak due to interactions of primary protons is clearly visible. The most striking feature is the large number of interacting neutrons at low energy. This feature can be easily explained, observing that charged particles start to be rapidly absorbed without further reinteractions, as soon as their range becomes comparable to the inelastic interaction length. This condition is fulfilled around 450 MeV for protons ($\text{range} \approx \lambda_I \approx 200 \text{ g cm}^{-2}$), and 200 MeV for pions in heavy materials. The importance of pions is quickly rising with the energy of the primary beam, since in high energy interactions pions are the most likely particles to be produced. The increasing importance of pions can be appreciated in fig. 11, where the same information of fig. 10 is presented for 15 and 150 GeV protons on uranium. It is also interesting to note the onset of kaon (and hyperon) production as well as of antinucleons.

Let's turn our attention to the energy deposition profiles: the large differences between Pb and U are mainly due to very different fission probabilities (see fig. 7). Indeed only a fraction of high energy particles can induce fissions in lead, ≈ 0.1 fissions per primary proton in this example, while ≈ 28 fissions occur in the uranium target, out of which ≈ 7 are due to energetic particles and ≈ 21 to neutrons below 20 MeV. As a result the uranium target is strongly exoenergetic: please note that also the EM energy deposition is strongly boosted due to the large number of neutrons, and hence of capture photons, produced because of these fissions. However such large differences are only apparent. The same physical mechanisms are at work in both cases, and will be explained in the next sections. The ridge in the hadronic energy deposition around the beam axis is just due to the primary beam ionization plus heavy recoils (\rightarrow short ranges) due to primary interactions, and to the most energetic particles emerging from inelastic interactions which are still strongly forward peaked. The higher values for U also in this region are due again to fissions occurring during primary interactions. The EM component can better be commented looking at the lead data, which are not masked by fissions. Two components can be identified: the first is due to π^0 decays and is concentrated again around the beam axis. This is due to the spatial scale of EM cascades, which is given by the radiation length (see paragraph 4) in the longitudinal direction, and by the Molière radius in the radial one. In medium and heavy materials both are much shorter than the "natural" hadronic length scale, given by the nonelastic interaction length. The second component is less intense but much more spread out, and it is given by photons locally produced by neutron reactions (capture, (n,n') etc). Of course this component is following the neutron pattern: the reason why it appears to be more extended in lead than the hadronic energy density, despite we claim it is due to neutron produced photons, is just that pure lead is a very bad moderator, but does not absorb too much neutrons. Therefore low energy neutrons are slowly moderated and diffuse much further away from the beam axis, depositing a small amount of hadronic energy through recoils, but a substantial amount of EM energy when captured.

Summarizing, what can be learned from these simple examples?

- a) Energetic particles (often called *shower* particles) are concentrated mainly around the pri-

mary beam axis, regardless of their identity. Their dE/dx and the EM cascades associated with π^0 constitute the “core” of the energy profiles.

- b) Neutral particles (\rightarrow neutrons, since these are the only neutral hadrons with enough long lifetime) dominate at energies such that charged particle ranges become shorter than the interaction length. The energy deposition associated with “low” energy neutron interactions, both recoils and photons, constitute the long tails in the energy deposition profiles.
- c) Most of the interactions are due to particles (mainly neutrons) of moderate energy, \rightarrow a good description of this energy range is mandatory.
- d) On the contrary the longitudinal shower development is ruled by *shower* particles, which carry a good fraction of the energy and have a longer interaction length. Taking also into account that any approximation or inaccuracy in the first interactions cannot be recovered with a better physics in the following ones, this means that a good description of energetic particle interactions is also mandatory.
- e) Pions can be only produced by *shower* particle interactions, so they are the real “tracer” of the high energy cascade. Neutrons and to less extent protons are copiously produced also in the final (evaporation) stages of nuclear interactions down to projectile energies comparable with their nuclear binding energy.

The term *shower* particles comes from the early experiments of high energy physics, where nuclear emulsions were often used as recording media. Charged particle tracks are therefore customarily classified in weakly ionizing, or *shower* tracks, medium ionizing, or *grey* tracks, and heavily ionizing, or *black* tracks, just according to their ionization rate (see the next section for a description of charged particles ionization). In practice, *shower* tracks correspond to (charged) particles with $\beta = \frac{v}{c} \geq 0.7$, *grey* tracks to $0.25 \leq \beta < 0.7$, and *black* tracks to $\beta < 0.25$. Forgetting the original meaning, but just retaining their velocity interval interpretation, such definitions are sometimes used also for neutral particles. $\beta = 0.7, 0.25$ corresponds to ≈ 400 MeV and 30 MeV for nucleons, and to ≈ 50 and 5 MeV for pions. Therefore black tracks are a good indicator of evaporation products.

3 Hadronic Showers

Actually hA cross sections at intermediate and high energies resemble the behaviour of the corresponding hN ones (see figs. 12 and 13), and this is not unexpected due to the strong relationship between σ_{hA} and σ_{hN} (see for example the discussion in [14] about the Glauber model of hadron-nucleus scattering). The main differences are in the resonance region, where cross section features are smoothed by the nucleon Fermi motion, and at very high energies where the increase of hA cross sections is slower than the corresponding hN ones. This feature can be easily explained in the Glauber model, observing that both total and absorption cross sections are determined by the probability of having at least one collision in the corresponding multiple

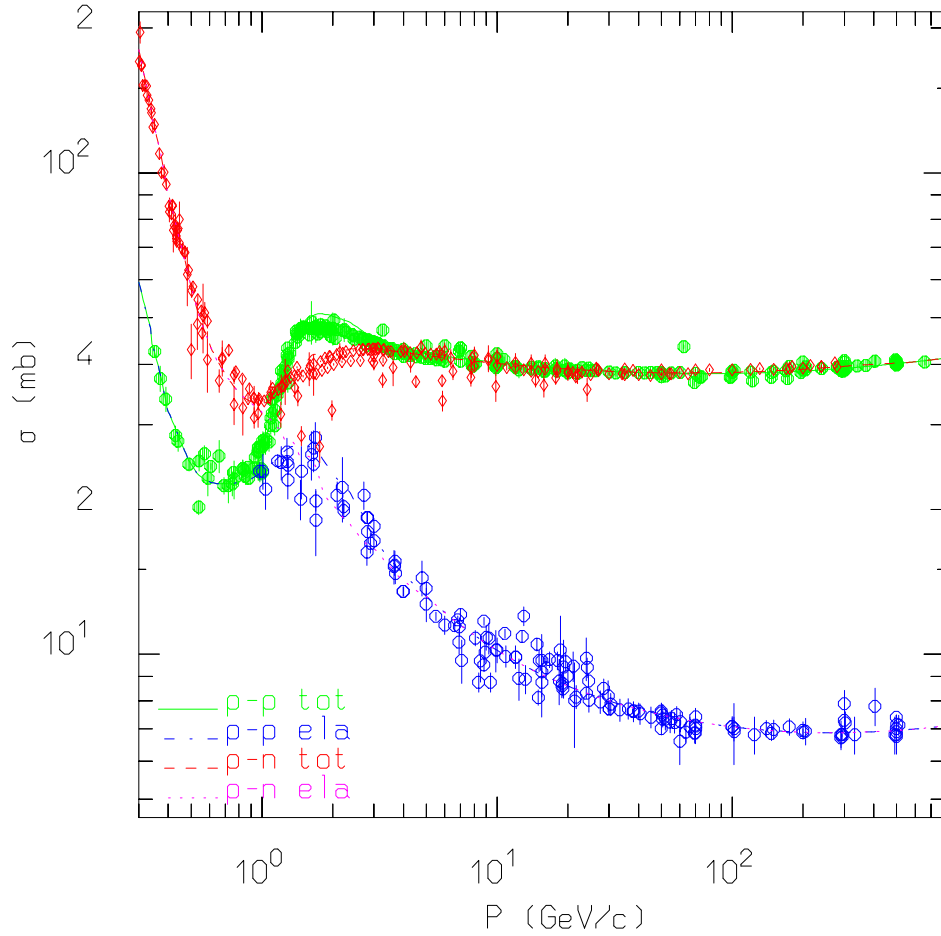


Figure 12: Total and elastic cross section for p–p and p–n scattering, together with experimental data

scattering expansions. Moderate increases in the elementary hN cross section are therefore effective only for large impact parameters where this probability is small, while for more central collisions they simply result in an increase of the average number of collisions rather than in an increase of the cross section. Typical behaviours of cross sections for neutrons on Copper and for negative pions on Carbon are reported in figs. 14 and 15, together with some representative experimental data.

It is customary to introduce a *nuclear interaction length*, λ_I , defined as the inverse of the macroscopic (reaction) cross section for several tens of GeVs protons or neutrons (the hA cross section above a few GeV varies very mildly with energy and can be assumed to be constant up to several hundred GeVs).

$$\lambda_I = \frac{P_a}{\sigma_{reac}\rho N_{av}} \quad (1)$$

where σ_{reac} is the microscopic reaction cross section, P_a the atomic weight, ρ the density, and N_{av} the Avogadro's number. The interaction length is the natural length scale for the longitudinal

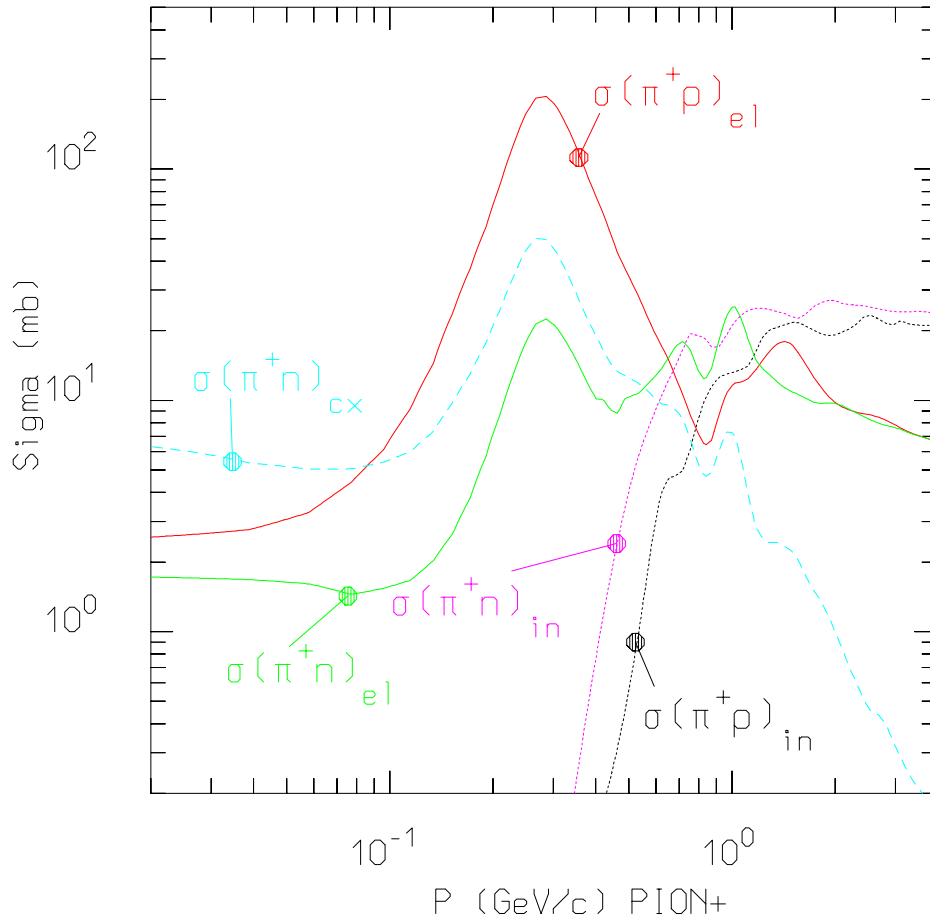


Figure 13: Cross sections for $\pi^+ p$ and $\pi^+ n$ reactions

development of the bulk of hadronic showers. The deep attenuation behaviour (mostly in the lateral direction) is however eventually dominated by the attenuation of neutrons in the 100-200 MeV region, for which the reaction cross section is at minimum.

4 ElectroMagnetic Showers

As soon as the primary beam energy exceeds the pion production threshold, an increasing fraction of the beam energy is dissipated through electromagnetic cascades, thanks to the production of neutral pions which almost immediately decays into two photons.

In first approximation and for high energy cascades, the fraction of the initial energy that goes into the electromagnetic sector is [18]

$$f_{EM} = 1 - \left(\frac{E}{E_0}\right)^{(\alpha-1)} \quad \alpha \approx 0.8 \quad E_0 \approx 1 \text{ GeV} \quad (2)$$

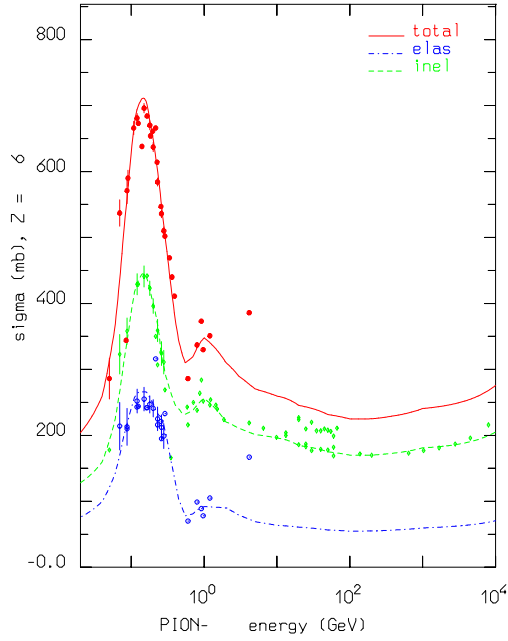


Figure 14: Total, elastic and inelastic cross section for negative pions on Carbon

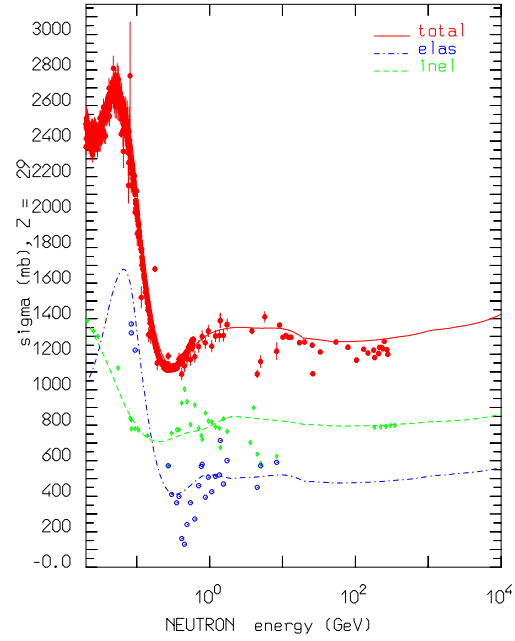


Figure 15: Total, elastic and inelastic cross section for neutrons on Copper

where the above equation has been derived assuming that at sufficiently high energy a constant fraction of the energy carried by a particle initiating a nuclear interaction goes into π^0 production.

In the following a simple introduction to EM cascades will be also given, assuming that the basic interactions of electrons and photons with matter are already known.

Let us consider an electron, or positron, of quite high energy, say a few hundreds of MeV, traversing a slab of material. It will lose energy mainly by bremsstrahlung, thus producing photons. For photons with energy higher than several MeV, the dominant interaction is pair production, thus most bremsstrahlung photons will produce an electron and a positron, and so on, building up what is called the EM shower [19, 20]. The shower will continue until the energy of its charged particles becomes low and they start to dissipate most of the energy in ionization. The distance traversed by the shower is most conveniently measured in *radiation lengths* X_0 . The radiation length is the distance over which an electron energy is reduced to e^{-1} of the initial one by bremsstrahlung emission. The radiation length is given by

$$\frac{1}{X_0} = 4\alpha r_e^2 \frac{N_A}{A} \left[Z^2 (\ln(184.15 Z^{-\frac{1}{3}}) - f_c(Z)) + Z \ln(1194 Z^{-\frac{2}{3}}) \right] \quad (3)$$

where $f_c(Z)$ is the Coulomb correction[21, 22]. An easy-to-use expression for X_0 is :

$$X_0 = \frac{716.4A}{Z(Z+1) \ln(287/\sqrt{Z})} \frac{g}{\text{cm}^2} \quad (4)$$

Another characteristic quantity is the critical energy E_c , defined as the energy at which the collision energy loss becomes equal to the radiation energy loss. It can be approximated by

$$E_c = \frac{1600}{Z} mc^2 \quad (5)$$

The longitudinal development of the shower cannot be calculated analytically, but a simple toy model can help in understanding its gross features: let us assume that each particle, electron or positron or photons, travels a length X_0 before interacting, and that e^\pm lose one half of their energy at each interaction, and each created lepton in pair production carries one half of the photon energy. Moreover, let us neglect collision energy loss above E_c , and conversely neglect radiation energy losses below E_c . This means that at each radiation length the number of particles in the shower is multiplied by two. After n radiation lengths there will be $N(t) = 2^t$ particles, each carrying an average energy $E_t = \frac{E_0}{2^t}$. At a certain depth t_c , the shower stops its development because the average particle energy equals the critical one: $\frac{E_0}{2^{t_c}} = E_c$. This happens at $t_c = \frac{\ln(E_0/E_c)}{\ln 2}$, that is, the maximum shower depth decreases logarithmically with energy. This simple model is in qualitative agreement with more refined ones; obviously the shower does not stop abruptly at t_c , but decreases gradually.

The lateral development of the shower scales with what is called the *Molière radius* R_M . This can be derived from a gaussian approximation to the Molière multiple scattering distribution: the width of this gaussian distribution for unit charge particles is

$$\theta_0 \approx \frac{\sqrt{\frac{4\pi}{\alpha}} m_e c^2}{\beta c p} \sqrt{\frac{x}{X_0}} \quad (6)$$

where βc and p are the projectile velocity and momentum. The lateral size of the shower at the shower maximum, ($E = E_c$) can be estimated by assuming that the particles will travel one radiation length before interacting or stopping. The width of the angular deflection will be given by

$$\theta_c = \frac{E_s}{E_c}; \quad E_s = \sqrt{\frac{4\pi}{\alpha}} m_e c^2 \quad (7)$$

and the radial width after a path X_0 , that is the Molière radius becomes:

$$R_M = \frac{E_s}{E_c} X_0 = 21.2 \frac{X_0}{E_c} \quad (8)$$

From measurements of the shower cascades, it turns out that only 10% of the energy lies outside the radius R_M .

5 Hadronic Showers: examples of scaling and spectral universality

As an example of hadronic showers, the fluences of various particles due to proton beams of 1, 10 and 100 GeV on infinite targets of Pb and polystyrene (CH) have been computed and compared. The target materials have been chosen as an example of a heavy (Pb) and light (CH) material respectively. The nuclear interaction, λ_I , and radiation, X_0 , lengths for Pb are 16.3 cm (185 g/cm²) and 0.56 cm (6.37 g/cm²) respectively. The corresponding numbers for CH are 76.3 cm (79.7 g/cm²) for λ_I , and 41.9 cm (43.8 g/cm²) for X_0 .

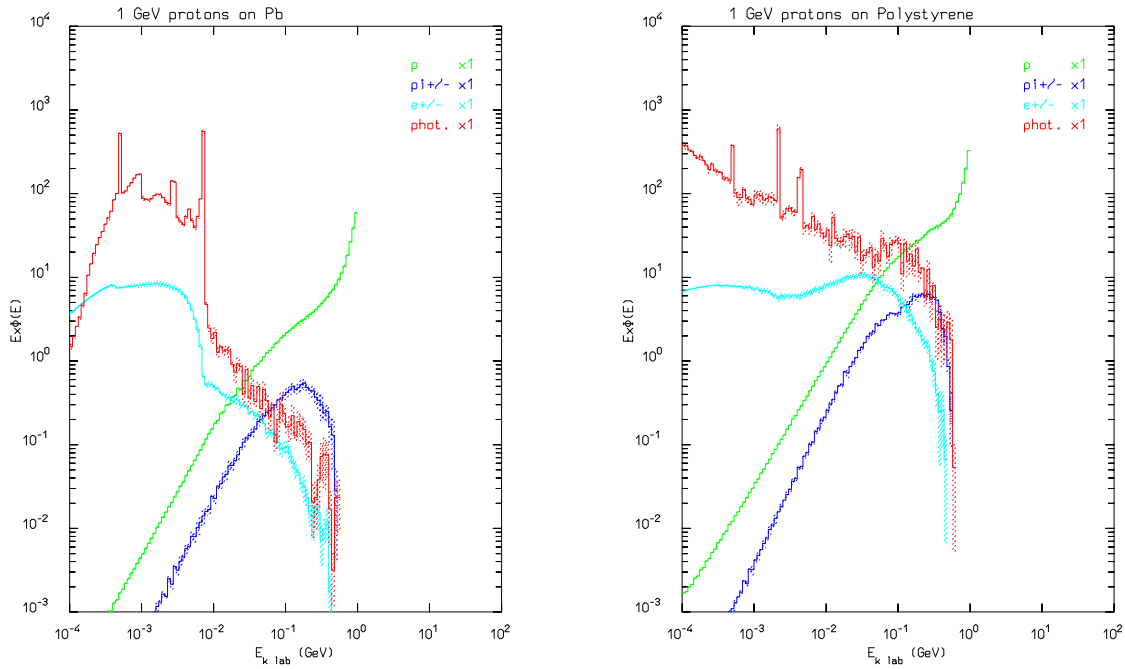


Figure 16: Proton, charged pion, electron and positron, and photon fluences for a 1 GeV proton beam hitting an infinite Lead (left) or Polystyrene (right) target

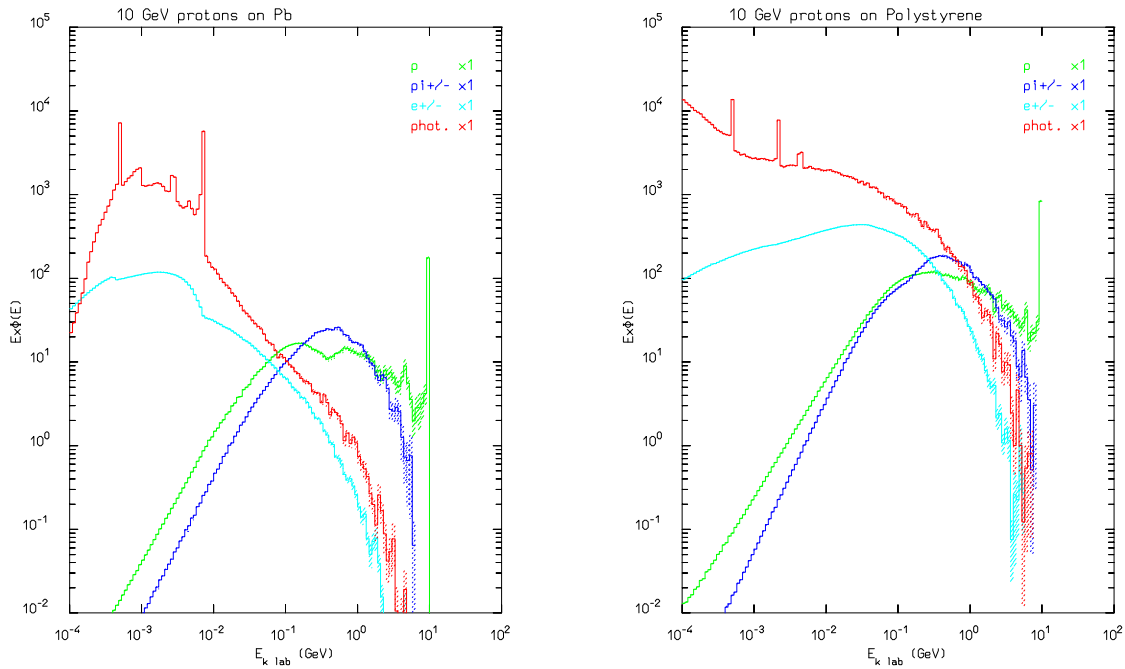


Figure 17: Proton, charged pion, electron and positron, and photon fluences for a 10 GeV proton beam hitting an infinite Lead (left) or Polystyrene (right) target

Proton, pion, electron/positron and photon fluences for both the Pb and CH targets are reported in figs. 16, 17, and 18 for the 1, 10, and 100 GeV cases respectively. Neutron fluences are presented in fig. 19 for the three energies together.

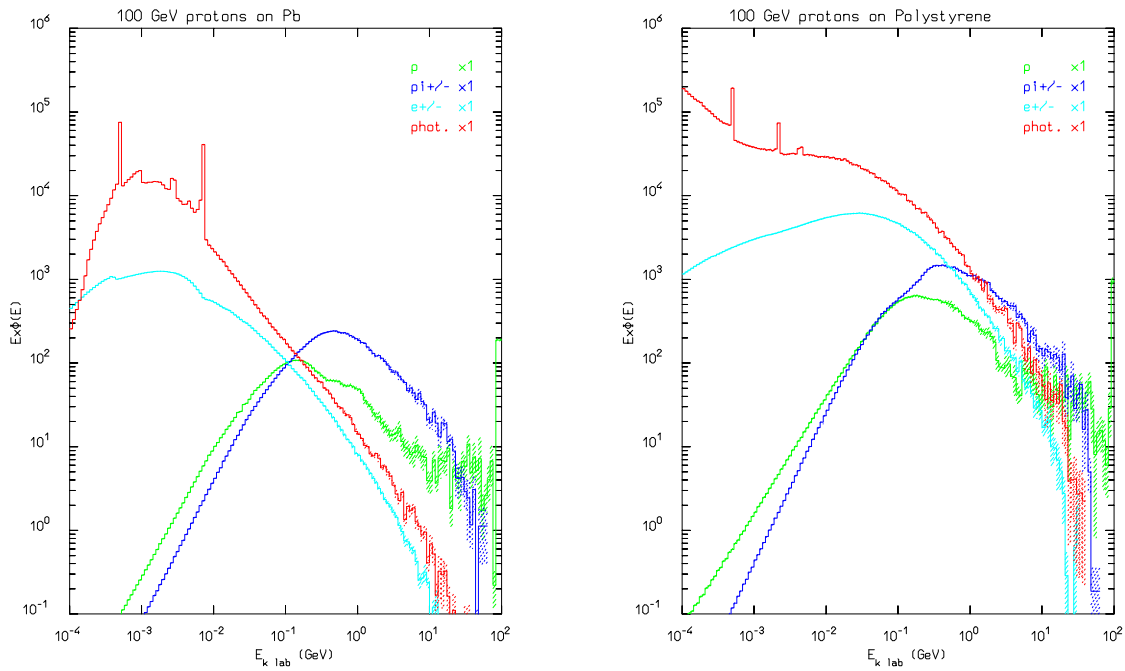


Figure 18: Proton, charged pion, electron and positron, and photon fluences for a 100 GeV proton beam hitting an infinite Lead (left) or Polystyrene (right) target

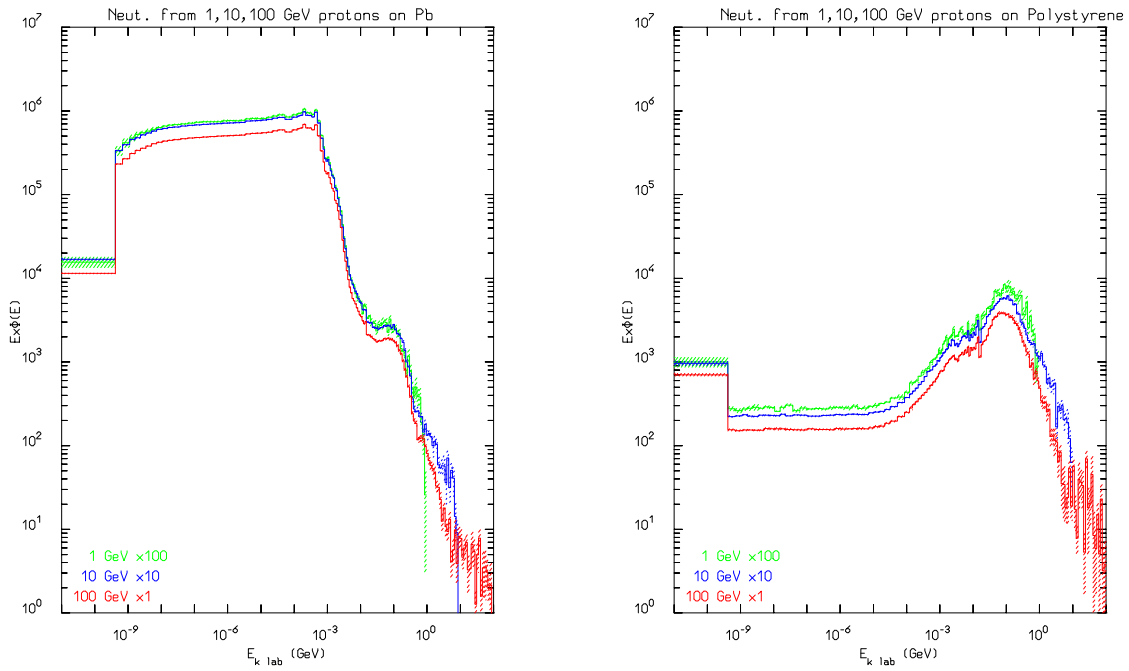


Figure 19: Neutron fluences for 1, 10 and 100 GeV proton beams hitting an infinite Pb (left) or Polystyrene (right) target

First of all some remarks about the hadronic particle fluences (protons, pions and neutrons), can be derived from these plots. Before starting the real discussion it is important to remind that

one of the many possible definitions of fluence is:

$$\Phi = \frac{dl}{dV} \quad (9)$$

where l is the particle tracklength and V the volume. Under the naive assumption that the hadronic component of showers scales with the interaction length, one would expect that at each energy the Pb and CH spectra can be brought into agreement simply multiplying the former one by $\frac{76.3}{16.3} \approx 5$, that is assuming that particle track length distributions are the same when expressed in interaction length units. An inspection of figs. 16, 17, and 18, shows that this assumption is roughly verified at 1 GeV (within a factor 2–3) and well verified at 100 GeV. This is not surprising since the interaction length is defined as the inverse of the macroscopic reaction cross section for protons/neutrons of several tens of GeV energy. However the rough scaling of hadron spectra with λ_I is very important and shows that, provided the energy is large enough, there are substantial similarities in the particle production mechanisms for targets as different as Pb and CH. It is also interesting to see how the pion component overcomes the proton one (despite the incident beam is a proton one), as soon as the primary energy exceeds a few GeVs.

Let's turn our attention to photons (and electron/positrons): two components are clearly apparent in the photon spectra:

- “Low” energy photons produced by neutron interactions (mostly captures) which extend up to a maximum of 7–8 MeV. This component is material specific and indeed the 2.2 MeV line of ${}^1H(n, \gamma){}^2H$ in the CH spectra and the over 7 MeV line of ${}^{207}Pb(n, \gamma){}^{208}Pb$ in the Pb one. Both spectra show the 0.511 MeV annihilation line as expected, and the electron/positron spectra at 1 and 10 GeV show clear signs of the Compton shoulders due to the capture lines. These photons due to neutron interactions scale with the energy like the hadronic components and therefore like E^α , $\alpha \approx 0.8$ as explained in section 4 (see also the discussion on neutron spectra in the following). The low energy part of the photon spectra is strikingly different in the two materials, and reflect the different behaviour of the photoelectric cross section which is already important in Pb at several hundred keVs while it is still negligible for CH.
- A continuum which extends up to high energies due to EM showers induced mainly by π^0 s production. These showers develop according to the radiation lengths which stand in the ratio $\frac{41.9}{0.56} \approx 60$. Indeed the photon and electron/positron spectra above the critical energies are in the ratios expected from the radiation lengths of the two materials. However the spectra for CH slow down their increase towards the lowest energies much before due to the much larger critical energy. The overall intensity of EM showers scales slightly faster than linear with the projectile energy according to our qualitative discussion in section 4.

Finally the neutron spectra have to be discussed and interpreted. The neutron spectra for three energies for Pb and CH are shown in fig. 19. A first important remark is that the spectra at the three different primary energies are almost identical in shape and scale almost linear in intensity with the incident energy, with the highest energy giving the lowest neutron yield per incident GeV, as predicted by our discussion in section 4. The low energy part of the spectra in

CH is completely different from the one in Pb, reflecting the different moderation (very effective in CH, very poor in Pb) and absorption properties of the two materials. The high energy part exhibits for both material the expected peak around ≈ 100 MeV, and the intensity scales with the material in a ratios which is somewhat lower than the λ_I ratio. This is due to the dominance of 100-200 MeV neutrons, whose attenuation properties are not well described by λ_I , since at those energies the cross section is somewhat different, elastic scattering cannot be neglected for light materials, and the number of cascade neutrons per interaction is larger for Pb than for CH.

The findings resulting from these simple examples can be summarized as follows:

- The hadronic component fluences, but low energy neutrons, roughly scale with the material according to λ_I , and with the primary energy with a power slightly less than one for primary energies in excess of 1 GeV.
- The low energy neutron component is strongly dependent on the material both for moderation and absorption, and scale with the primary energy with the same power of the “fast” hadronic component.
- As a consequence of the previous two points, the overall neutron spectrum, while being material specific in its low energy component, is practically (primary) energy independent in shape and scales close to linear with the primary energy.
- The EM component fluences above the critical energy, scale with the material according to X_0 , and almost linearly with the primary energy.
- The low energy (below one binding energy, ≈ 8 MeV) photon fluence (and hence the electron one) has a substantial contribution from neutron interactions (mainly captures). It is therefore material specific and scales with primary energy like the low energy neutron component.

6 (Generalized)IntraNuclear Cascade

Hadron-nucleus non-elastic interactions in the energy range of interest for high energy showers can be described mostly in the framework of the IntraNuclear Cascade (INC) model. This model was developed at the very beginning (the original ideas go back at the end of the 40’s) of the history of energetic nuclear interaction modelling, but it is still very valid and in some energy range it is the only available choice. The model is intrinsically a MonteCarlo model, well suited for numerical applications, while no closed analytical expression can be derived without severe approximations. Therefore INC models became more and more refined and widespread with the evolution of computer codes; currently available models can reach 100,000 lines of program.

In the energy range going from the pion production threshold (≈ 290 MeV for a free nucleon, down to 200 MeV for nucleons in nuclei because of the Fermi motion) to high energies, INC models are practically the only available tools to model hadron-nucleus interactions. At lower

energies, a variety of preequilibrium models can do a very good job, with physics foundations which become surely more robust than those of INC ones as the energy is going down.

One of reasons of the long dating success of INC models is their ability to model in reasonable time, almost whichever target nucleus with whichever projectile, with no or small need for external input informations or preliminary calculations. The other great advantage is that all correlation among the different quantities and particles are fully reproduced.

6.1 Basic assumptions of IntraNuclear Cascade (INC) models

Classical INC codes [23, 24, 25, 26] are based on a more or less accurate treatment of hadron multiple collision processes in nuclei, the target being assumed to be a cold Fermi gas of nucleons in their potential well [27, 28]. The hadron-nucleon cross sections used in the calculations are free hadron–nucleon cross sections. Usually, the only quantum mechanical concept incorporated is the Pauli principle. Possible hadrons are often limited to pions and nucleons, pions being also produce or absorbed via isobar (mainly Δ_{33}) formation, decay, and capture. The Fermi motion is taken into account when considering elementary collisions, both for the purpose of computing the interaction cross section, and to produce the final state particles. The basic assumptions of INC models can be summarized as follow:

1. Hadrons propagate like free particles in the nuclear medium, with interaction probability per unit length given by free space cross sections, properly averaged over the Fermi motion of the target nucleons, times the local nuclear density.
2. The particle motion is formulated in a classical way. It can be subject to an average nuclear mean potential, which must be added to the free particle kinetic energy when tracking through the nucleus. The radial and energy dependence of such field are model and particle dependent.
3. The effect of the nuclear mean field on the particle motion can either be null or can produce curved trajectories in a semiclassical approach, according to energy and momentum conservation, depending on the model. The curvature effects induced by the nuclear mean field are usually referred to as refraction and reflection effects.
4. Interactions occur like in free space in the Center of Mass System of the two colliding hadrons. Of course, because of the Fermi motion, the lab frame will not coincide with the frame where the target nucleon is at rest, but suitable Lorentz boosts have to be applied to transform back the secondary particles in the lab frame.
5. Interactions occur in a completely incoherent and uncorrelated way. No coherence or diffractive effect is included. No multibody or cluster process is included, with the possible exception of pion absorption (see next sections).
6. Quantum effects are mainly limited to Pauli blocking (see ref. [14] for more details): only few codes contain further quantum effects (see again [14] for a discussion).

7. Secondaries are treated exactly like primary particles, with the only difference that they start their trajectory already inside the nucleus.

An obvious requirement arising from the previous points is that the wavelength associated to hadron motion must be much shorter than the hadron mean free path inside the target nucleus, and also much shorter than the average distance among two neighboring nucleons. That is:

$$\lambda_h = \frac{2\pi\hbar}{p} \ll \frac{1}{\sigma_{hN}\rho} \quad (10)$$

$$\lambda_h = \frac{2\pi\hbar}{p} \ll \left(\frac{3}{4\pi\rho}\right)^{1/3} \quad (11)$$

The nucleon density at the center of nuclei is typically $\rho \approx 0.17 \text{ fm}^{-3}$, therefore the latter condition would require a particle momentum in excess of 1 GeV/c. For a projectile nucleon, again at central density, the former condition is fulfilled only starting from 200 MeV (see fig. 12 for evaluating σ_{hN}). From these back of the envelope estimates it would appear that INC models cannot work at all, unless the projectile energy is above a few hundreds MeV. Furthermore, the transport and reinteraction inside the nucleus of secondary particles, which are at lower energies, cannot easily comply with the above requirements. Fortunately the situation is not so bad as it could appear. Pauli blocking and other effects contribute to increase particle mean free paths. In particular Pauli blocking is more effective for low energy particles, thus partially compensating the increase in nucleon-nucleon cross sections at low energies. Furthermore, hadronic interactions are mostly surface effects (as can be easily checked both from mean free paths and realizing that hadron-nucleus cross sections scale with the target atomic mass approximately like $A^{2/3}$). Hence the nuclear reactions mostly occur at densities significantly lower than the central one, therefore partially mitigating the requirements on particle energies. However it is clear that the physical foundations of INC are not very sound for primary or secondary particle momenta below a few hundreds of MeV/c. According to these considerations, the quality of results which can be obtained by INC codes is somewhat surprising.

However plain INC models like those developed in the seventies become unreliable both at the lower ($< 100\text{-}200 \text{ MeV}$) and higher ($> 2\text{-}3 \text{ GeV}$) ends of the energy scale, and show limitations also when used in the proper energy range.

Once suitable models for describing hadron-nucleon interactions are available, the high energy regime can be properly handled provided the spacetime characteristics of high energy interactions and multiple primary collisions according to the Glauber approach (see [14] and references therein) are taken into account. Models which includes these features are often referred to as *Formation Zone IntraNuclear Cascade* or *Glauber Cascade* approaches (see for example [29, 30]).

Important Changes to the original INC approach must be done also at the lowest energies, and are mainly related with quantum nuclear effects and multibody interactions, besides the introduction of a preequilibrium stage.

IntraNuclear Cascade approaches which make use both of the high energy and low energy extensions can be called (*Generalized*) *IntraNuclear Cascade* models, and will be referred as

such in the next sections.

The examples shown in the previous and next paragraphs have been computed using the (G)INC model implemented in the FLUKA code, whose low-medium energy part (up to few GeV) is called PEANUT (for PreEquilibrium Approach to Nuclear Thermalization).

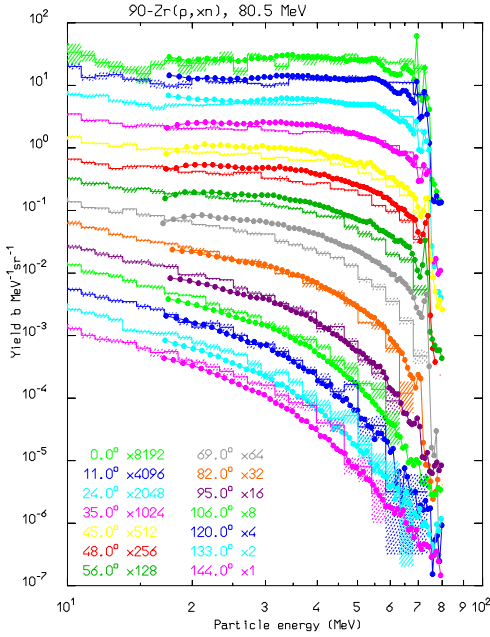


Figure 20: Double differential Zr(p,xn) spectra at 80.5 MeV for 14 different emission angles, PEANUT (histo) calculations and experimental data [42] (symbols)

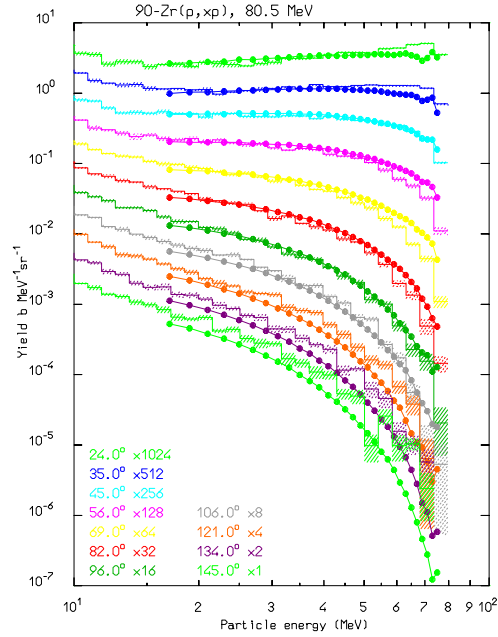


Figure 21: Double differential Zr(p,xp) spectra at 80.5 MeV for 11 different emission angles, PEANUT (histo) calculations and experimental data [43] (symbols)

6.2 The Steps of an INC simulation

A typical INC code usually follows the following logic:

- Target nucleus description, typically realized through a few concentric spheres of different density and Fermi energy
- Geometrical cross section, corresponding to the nuclear radius or to the maximum possible impact parameter
- Impact parameter selection with a constant probability over the geometrical cross section area. More than one selection can be required if the particle crosses the nucleus without interacting
- Interaction point selection and projectile tracking through the nucleus, according to Fermi motion averaged hadron-nucleon cross sections and possibly to the nuclear mean field, including the Coulomb field

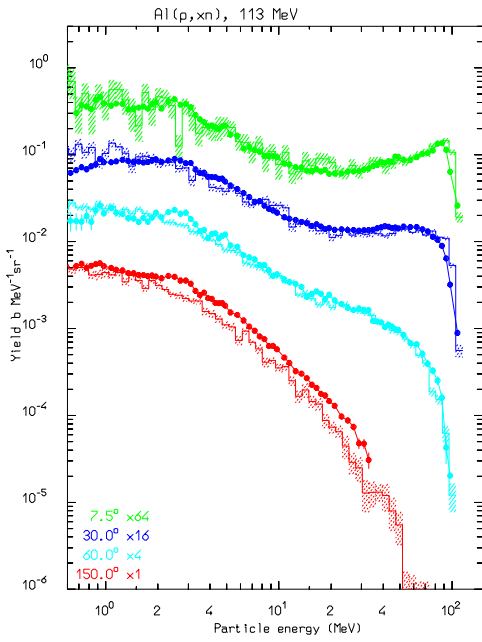


Figure 22: Double differential Al(p,xn) spectra at 113 MeV for 4 different emission angles, PEANUT (histo) calculations and experimental data [44] (symbols)

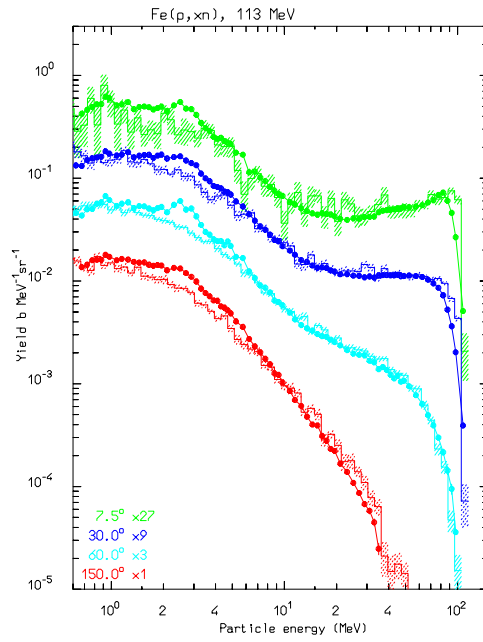


Figure 23: Double differential Fe(p,xn) spectra at 113 MeV for 4 different emission angles, PEANUT (histo) calculations and experimental data [44] (symbols)

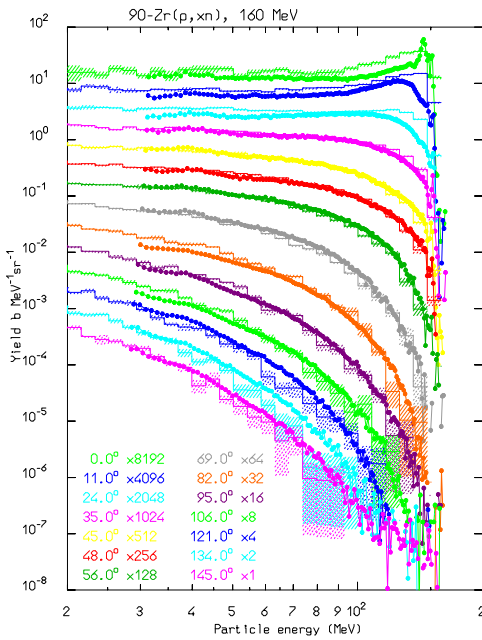


Figure 24: Double differential Zr(p,xn) spectra at 160 MeV for 14 different emission angles, PEANUT (histo) calculations and experimental data [45] (symbols)

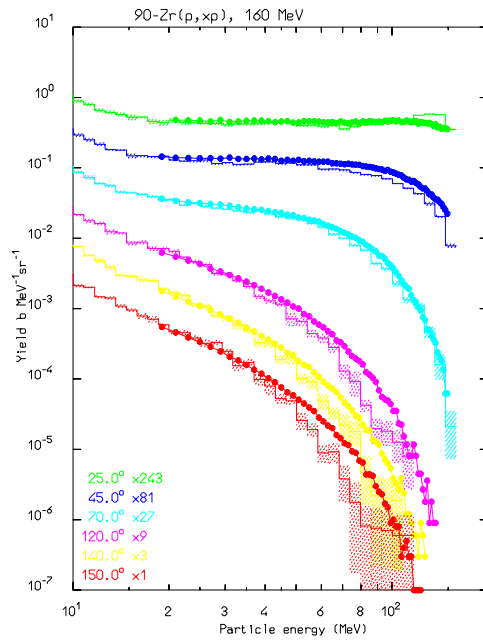


Figure 25: Double differential Zr(p,xp) spectra at 160 MeV for 6 different emission angles, PEANUT (histo) calculations and experimental data [46] (symbols)

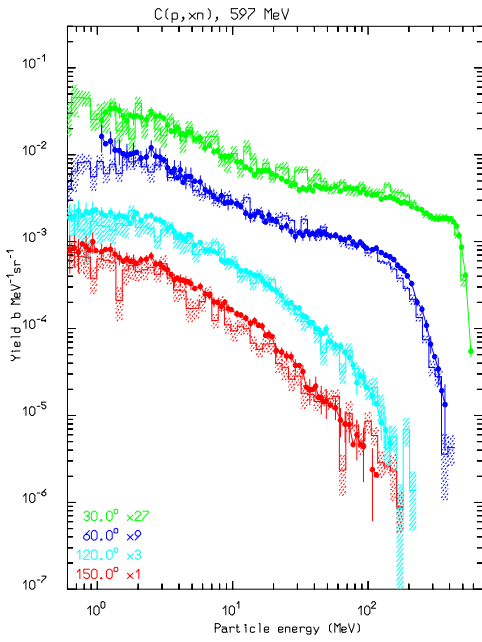


Figure 26: Double differential C(p,xn) spectra at 597 MeV for 4 different emission angles, PEANUT (histo) calculations and experimental data [47] (symbols)

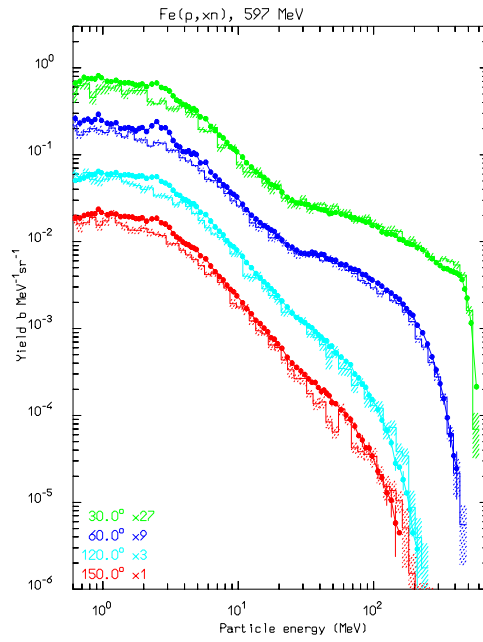


Figure 27: Double differential Fe(p,xn) spectra at 597 MeV for 4 different emission angles, PEANUT (histo) calculations and experimental data [47] (symbols)

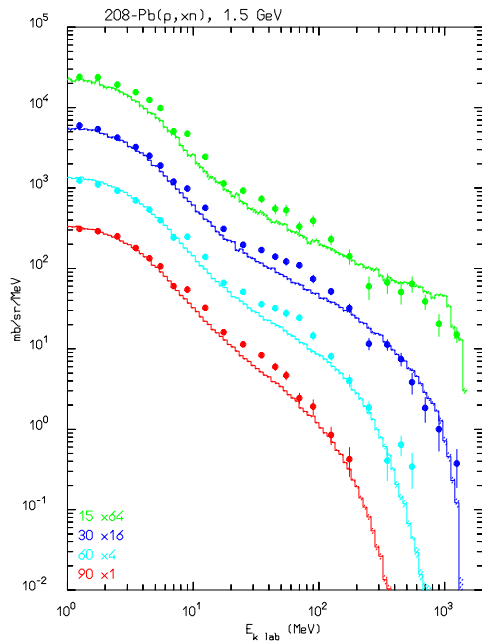


Figure 28: Double differential Pb(p,xn) spectra at 1.5 GeV for 4 different emission angles, PEANUT (histo) calculations and experimental data [48] (symbols)

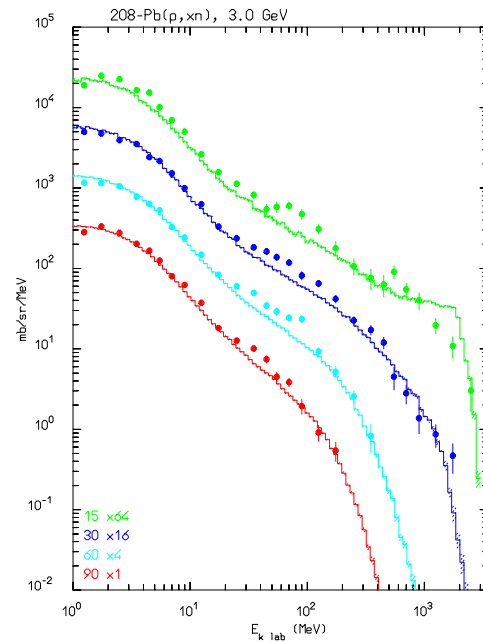


Figure 29: Double differential Pb(p,xn) spectra at 3.0 GeV for 4 different emission angles, PEANUT (histo) calculations and experimental data [48] (symbols)

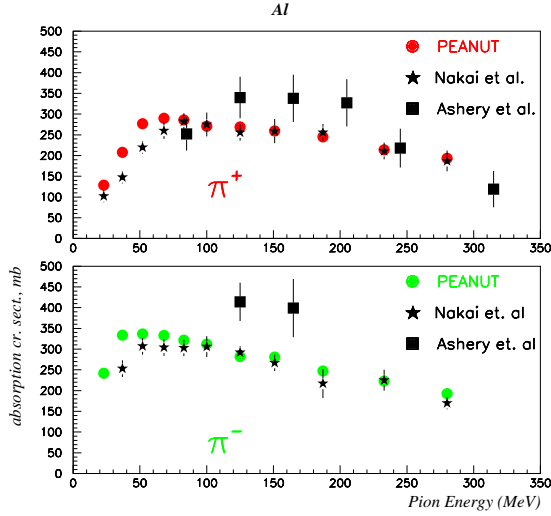


Figure 30: Pion absorption cross section on Aluminum as a function of energy, PEANUT (color symbols) calculations and experimental data [49, 50] (black symbols)

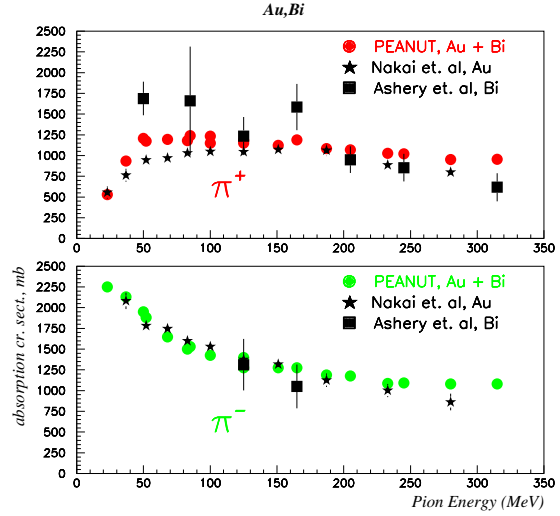


Figure 31: Pion absorption cross section on Gold or Bismuth as a function of energy, PEANUT (color symbols) calculations and experimental data [49, 50] (black symbols)

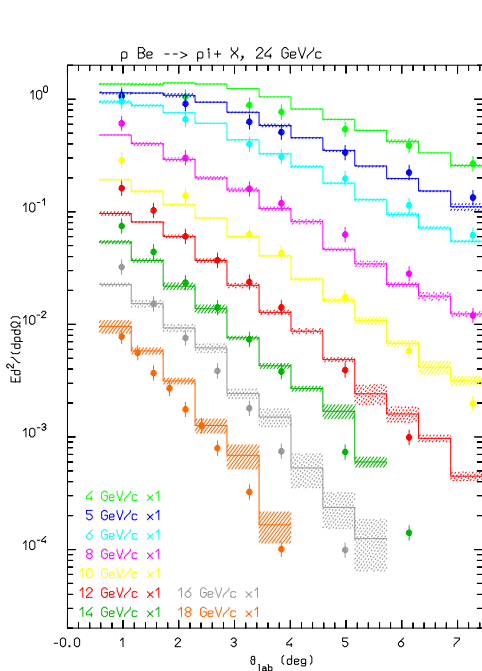


Figure 32: Double differential invariant $\text{Be}(p, X\pi^+)$ spectra at 24 GeV/c as a function of the emission angle for 9 different momenta, FLUKA (histo) calculations and experimental data [51] (symbols)

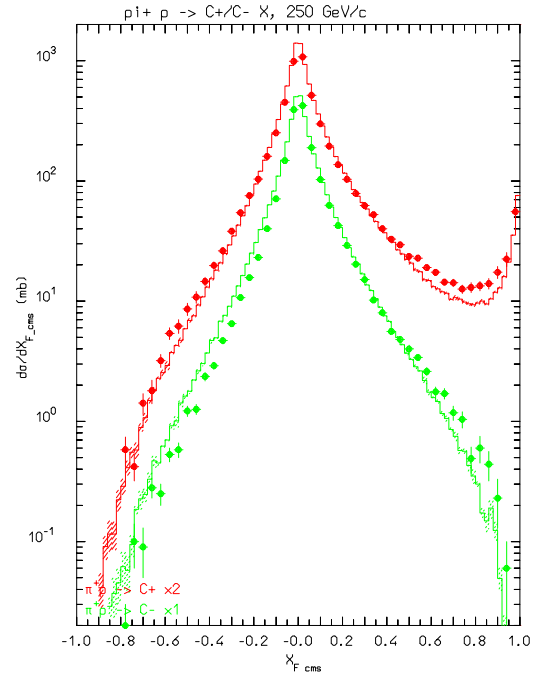


Figure 33: Feynman X_F^* spectra of positive particles and π^- produced by 250 GeV/c π^+ incident on a hydrogen target. Symbols are exp. data [52], the dashed histogram is the FLUKA result

- Target nucleon selection according to σ_{hp} , σ_{hn} and local Fermi energy
- Interaction simulation according to free hN interactions, local Fermi energy and Pauli blocking
- Secondary tracking into the nucleus, until interaction, escape, or energy cut-off
- (Possible) preequilibrium stage, whenever all excited nucleons are below a given energy threshold (typically a few tens of MeV). This stage is included only in the most recent developments
- Evaporation stage whenever the preequilibrium stage is finished, or all particles are below a given threshold (usually of the order of the binding energy), and the system can be assumed to be equilibrated
- Final deexcitation stage when the excitation energy is below the threshold for particle emission and it is spent through photon emission

A description of the physics involved in all stages can be found in [14]. It is important to remark that in principle INC codes are able to compute reaction cross sections by themselves. Indeed, the reaction cross section is given by the geometrical one times the probability of interaction. The latter information can be easily derived from the ratio of the impact parameter selections which gave rise to interactions and the total number of selected impact parameters.

6.3 Advantages and Limitations of INC models

A few of the strong points of INC codes have been already touched in the introduction to this section, however they are repeated here for completeness:

- No other model available for energies above the pion threshold (with the exception of QMD models, which however include a substantially similar approach for including hadron-nucleon nonelastic interactions)
- No other model for projectiles other than nucleons
- Easily available for on-line integration into transport codes
- Every target-projectile combination, without any extra information
- Particle-to-particle correlations preserved
- Equally valid on very light as well as on very heavy nuclei (with some question mark on evaporation)
- Capability of computing reaction cross section where unknown

Before going into details about weak points of INC codes, it must be remarked that many of the historical weaknesses have been mitigated or even completely solved in some of the most recent developments [31, 32, 33, 34, 35]. In the following list, points flagged with an asterisk refer to glorious but old models, typically the Bertini model [24, 36, 37], but are partially or completely solved in state-of-the-art codes.

- *Low projectile energies ($E \leq 100 - 200$ MeV) are badly described
- *Binding energy: the commonly used assumption of a constant binding energy makes the end points, shapes, and absolute intensities of emitted particle spectra increasingly meaningless for energies below 100 MeV, particularly for reactions like (p, xn) or (n, xp)
- *Backward angle emission poorly described
- *Coulomb barrier effect: neglected when refraction/reflection are not modelled or no Coulomb potential is included
- *Cross section calculations: crazy when no potential effect is included for $E < 100$ MeV, and anyway at low energies. This point is particularly critical for codes, like the original HETC [38], which make use of INC computed cross sections for particle transport
- *Secondary transport threshold: down to energies much lower than any safe limit for the theory
- Quasielastic peaks above 100 MeV are usually too sharp when compared with experimental data [39]
- Coherent effects as well as direct transitions to discrete states are not included
- Nuclear medium effects which can alter interaction properties are not taken into account
- Multibody processes, like interaction on nucleon clusters, are not included in INC approaches (with the possible exception of pion absorption)
- Composite particle emission (d, t, ^3He , α) cannot be easily accommodate into INC codes, but for the evaporation stage.

It must be stressed that a relevant part of the improvements achieved at the lowest energy end by recent developments is due to the inclusion of a preequilibrium stage, which prevents the INC part from working in an unsafe energy range, and strongly improves the modelling of reactions at the lowest energies. Since most of the interactions for a real shower occur in this energy range, it is highly questionable the use of codes which are still based on sloppy physics in this region.

7 A few Examples of INC calculations

In the previous sections, a brief introduction to the (G)INC approach for hadronic inelastic interactions has been given. In the present section, a few representative comparisons between model results and experimental data on particle production are presented, with particular emphasis on the intermediate energy range and secondary nucleon production. All the presented results have been obtained with the last version of the FLUKA [40, 41, 34] code, and more precisely with the model used for the intermediate energy range [32, 33, 34, 14] and called PEANUT (PreEquilibrium-Approach-to-NUclear-Thermalization). This model combines both an INC part, and a preequilibrium part, with a smooth transition around 50 MeV for secondary nucleons, and 30 MeV for primary ones. Nuclear potential effects (refraction and reflection) are modeled into the code, as well as quantistic effects, like Pauli blocking, nucleon-nucleon correlations, fermion antisymmetrization, coherence length and formation zone. The results obtained with this code are not representative of the majority of the INC models, usually based on some flavour of the Bertini INC code [24, 36, 37], or equivalent approaches. Among the available INC codes, possibly only those which include a preequilibrium model (i.e. CEM92 [35] and LAHET [31]) and possibly features like refraction and reflection and quantum effects can be compared with this model for nucleon induced interactions. For pion induced interactions, the approach of PEANUT is very different from most other codes, none of which includes a complex optical potential or absorption effects computed according to modern approaches [4, 6, 5] including three body absorption.

The presented examples can be summarized as follows:

- Double differential ($d^2\sigma/d\Omega dE$) distributions of outgoing neutrons/protons for nucleon induced reactions below the pion production threshold. Examples at 80, 113, and 160 MeV incident energies are reported in figs. 20, 21, 22, 23, 24, and 25. These examples show that, when coupled to a preequilibrium stage (G)INC models perform fairly well already at these relatively low energies.
- Double differential ($d^2\sigma/d\Omega dE$) distributions of outgoing neutrons for nucleon induced reactions above the pion production threshold. Examples at 597, 1500, and 3000 MeV incident energies are reported in figs. 26, 27, 28, and 29. These examples span an energy range and reaction products where most INC codes are fairly successful.
- Pion induced reactions: two examples only are reported, showing the pion absorption (no pion in the final state) cross section as a function of incident pion energy for positive and negative pions on Al (fig. 30 and Au/Bi (fig. 31). Pion absorption reactions are particularly important because of their large branching ratio in the Δ region and because they are a source of energetic nucleons. Furthermore they are a typical nuclear multibody effect, which is not present in pion-nucleon reactions.
- High energy examples: just one hadron-nucleus and one hadron-nucleon example are reported in figs. 32 and 33 respectively. The high energy range is fairly complex and does require significant efforts first of all in hadron-nucleon modelling and then in its extension to nuclear interactions.

Acknowledgments

The authors are greatly indebted to A. Fassò and J. Ranft for the many stimulating discussions and the continuous support. Part of this lecture is based on similar talks given at the 1995 “Frederic Joliot Summer School in Reactor Physics” [8], Cadarache 1995, and at the “Workshop on Nuclear Reaction Data and Nuclear Reactors Physics, Design and Safety” [14], Trieste 1996.

References

- [1] C. Birattari et al., *Measurements and simulations in high energy neutron fields*, Proceedings of the 2nd “Specialists’ Meeting on Shielding Aspects of Accelerators, Targets & Irradiation Facilities” (SATIF-2), CERN-Geneva October 12–13 1995, published by OECD/NEA, OECD documents, ISBN 92-64-15287-3 (1996), 171.
- [2] E. Gadioli and P. E. Hodgson, *Pre-equilibrium Nuclear Reactions* (Clarendon Press, Oxford, 1992).
- [3] R. Bonetti et al., *Phys. Rep.* **247** (1994) 1.
- [4] E. Oset and L.L. Salcedo, *Nucl. Phys.* **A468** (1987) 631.
- [5] M.J. Vicente Vacas and E. Oset, *Nucl. Phys.* **A568** (1994), 855.
- [6] L.L. Salcedo et al., *Nucl. Phys.* **A484** (1988) 557.
- [7] A. Ferrari and P. R. Sala, *Improvements to the Electromagnetic part of the FLUKA code*, to be published; P. A. Aarnio, A. Fassò, A. Ferrari, J. -H. Moehring, J. Ranft, P.R. Sala, G.R. Stevenson and J.M. Zazula, *Electron-photon transport: always so good as we think? Experience with FLUKA*, in Proc. of the “MC93 Int. Conf. on Monte Carlo Simulation in High-Energy and Nuclear Physics”, Feb. 22-26, 1993. Ed. P. Dragovitsch, S.L. Linn, M. Burbank, World Scientific, Singapore, 1994 (p. 100).
- [8] A. Ferrari and P.R. Sala, *Physics of Showers induced by Accelerator Beams*, in Proceedings of the “1995 Frederic Joliot Summer School in Reactor Physics”, August 22–30 1995, Cadarache, France, CEA ed., Vol. 4 (1996), Lecture 5b.
- [9] E.A. Uehling, *Ann. Rev. Nucl. Sci.*, **4** (1954), 315
- [10] H. Bethe, and J. Ashkin, *Passage of radiation through matter*, in E. Segre (ed.) *Experimental Nuclear Physics*, Vol. 1, Part 2, Wiley New York (1959).
- [11] U. Fano, *Ann. Rev. Nucl. Sci.*, **13** (1963), 1.
- [12] Int. Commission on Rad. Units and Measurements, *Stopping Powers for Electrons and Positrons*, ICRU Report **39** (1984).

- [13] Int. Commission on Rad. Units and Measurements, *Stopping Powers and Ranges of Protons and Alpha Particles*, ICRU Report **49** (1993).
- [14] A. Ferrari, and P.R. Sala, *The Physics of High Energy Reactions*, in Proceedings of the “Workshop on Nuclear Reaction Data and Nuclear Reactors Physics, Design and Safety”, International Centre for Theoretical Physics, Miramare-Trieste, Italy, 15 April–17 May 1996, World Scientific in press.
- [15] M. B. Emmett, *The MORSE Monte Carlo radiation transport code system*, Report ORNL-4972 (1975).
- [16] J.F. Briesmeister, editor *MCNP - A general Monte Carlo code for neutron and photon transport*, Los Alamos report **LA-7396-M Rev.2** (1986).
- [17] J.P. Both et al., in Proc. of the “8th International Conference on Radiation Shielding”, Arlington, April 24-28 1994, American Nuclear Society ed., Vol. 1 373 (1994).
- [18] T.A. Gabriel et al., Nucl. Inst. Meth. **A338** (1994) 336.
- [19] R. Fernow, *Introduction to experimental particle physics* Cambridge University Press, 1986.
- [20] Particle Data Group, *Review of Particle Properties*, Phys. Rev. **D50**, part 1, 1994.
- [21] Y.S. Tsai, Rev. of Mod. Phys., **46** (1975) 815.
- [22] H.A. Bethe and L.C. Maximon, Phys. Rev. **93** (1954) 768; H. Davies, H.A. Bethe, and L.C. Maximon, Phys. Rev. **93** (1954) 788.
- [23] N. Metropolis et al., Phys. Rev., **100(1)** (1958), 185; N. Metropolis et al., Phys. Rev., **100(1)** (1958), 204.
- [24] H.W. Bertini, Phys. Rev., **131(4)** (1963), 1801.
- [25] V.S. Barashenkov et al., Sov. Phys. Usp. **16(1)** (1973) 31; V.S. Barashenkov et al., Nucl. Phys **A222** (1974) 204.
- [26] K. Chen et al., Phys. Rev., **166** (1968), 949; K. Chen et al., Phys. Rev., **176** (1968), 1208.
- [27] R. Serber, Phys. Rev., **72** (1947), 1114.
- [28] M.L. Goldberger, Phys. Rev., **74** (1948), 1269.
- [29] A. Ferrari, P.R. Sala, J. Ranft, and S. Roesler, *Z. Phys.* C70, 413 (1996).
- [30] A. Ferrari, P.R. Sala, J. Ranft, and S. Roesler, *Z. Phys.* C71, 75 (1996).
- [31] R.E. Prael and M. Bozoian, Los Alamos report **LA-UR-88-3238** 1988.

- [32] A. Ferrari, and P. R. Sala, in Proc. of the “MC93 Int. Conf. on Monte-Carlo Simulation in High-Energy and Nuclear Physics”, Tallahassee, Florida, 22-26 february (1993), World Scientific ed. (1994), 277; A. Fassò, A. Ferrari, J. Ranft, and P. R. Sala, in Proc. of the “Specialists’ Meeting on Shielding Aspects of Accelerators, Targets & Irradiation Facilities”, Arlington, April 28-29 1994, published by OECD/NEA (1995), 287; A. Fassò, A. Ferrari, J. Ranft, and P. R. Sala, in *Intermediate Energy Nuclear Data: Models and codes*, Proc. of a specialist’ meeting, Issy-les-Moulineaux, May 30th - June 1st 1994, published by OECD/NEA (1994), 271.
- [33] A. Fassò, A. Ferrari, J. Ranft and P.R. Sala, in Proc. of the 2nd workshop on “Simulating Accelerator Radiation Environment”, SARE-2, CERN-Geneva, October 9–11 1995, CERN Divisional report CERN/TIS-RP/97-05 (1997), p. 158.
- [34] A. Fassò, A. Ferrari, J. Ranft and P.R. Sala, *New developments in FLUKA modelling of hadronic and EM interactions*, in Proc. of the 3rd workshop on “Simulating Accelerator Radiation Environment”, SARE-3, KEK-Tsukuba, May 7–9 1997, in press.
- [35] S.G Mashnik and S.A. Smolyansky, JINR preprint E2-94-353 , Dubna (1994).
- [36] H.W. Bertini, Phys. Rev., **C1(2)** (1970), 1801.
- [37] H.W. Bertini, Phys. Rev., **6(2)** (1972), 631.
- [38] K.C. Chandler, and T.W. Amstron, *Operating instructions for the high-energy nucleon-meson transport code HETC*, ORNL-4744 (1972); K.C. Chandler, and T.W. Amstron, Nucl. Sci. and Eng., **49** (1972), 110; R.G. Alsmiller, F.S. Alsmiller and O.W. Hermann, Nucl. Instr. Meth., **A295** (1990), 337.
- [39] *International Code Comparison for Intermediate Energy Nuclear Data*, M. Blann, H. Gruppelaar, P. Nagel and J. Rodens eds., OECD/NEA (1994).
- [40] A. Fassò, A. Ferrari, J. Ranft, P. R. Sala, G. R. Stevenson, and J. M. Zazula, in Proc. of the workshop on “Simulating Accelerator Radiation Environment”, SARE, Santa Fè, 11-15 january (1993), A. Palounek ed., Los Alamos LA-12835-C (1994), 134.
- [41] A. Fassò, A. Ferrari, J. Ranft and P. R. Sala, in Proc. of the “IV International Conference on Calorimetry in High Energy Physics”, La Biodola (Elba), September 19-25 1993, A. Menzione and A. Scribano eds., World Scientific (1994), 493.
- [42] M. Trabandt et al., Phys. Rev., **C39** (1989), 452.
- [43] A.A. Cowley et al., Phys. Rev., **C43** (1991), 678.
- [44] M.M. Meier et al., Nucl. Sci. and Eng., **102**, (1989), 310.
- [45] W. Scobel et al., Phys. Rev., **C41** (1990), 2010.
- [46] W.A. Richter et al, NAC Annual report, **92-01** (1992).
- [47] W.B. Amian et al., Nucl. Sci. Eng., **115** (1993), 1.

- [48] K. Ishibashi et al, Nucl. Sci. Technol., **32** (1995), 827.
- [49] K. Nakai et. al. Phys. Rev. Lett., **44** (1979), 1446.
- [50] D. Ashery et al., Phys. Rev., **C23** (1981), 2173.
- [51] T.Eichten et al., Nucl. Phys., **B44** (1972), 333.
- [52] M. Adamus, Z. Phys., **C39** (1988), 311.